# A novel model and design of a MEMS Stirling cooler for local refrigeration

Sylvie Bégot, Muluken Zegeye Getie, Alpha Dassimou Diallo, François Lanzetta, Magali Barthes, Michel de Labachelerie

# A novel model and design of a MEMS Stirling cooler for local refrigeration

*Sylvie* Bégot[1,*], *Muluken* GETIE[1,2], *Alpha* Diallo[3], *François* Lanzetta[1], *Magali* Barthès[3], *Michel* de Labachelerie[3]

[1]FEMTO-ST Institute, Univ. Bourgogne Franche-Comte, CNRS, Energy Department, Parc technologique, 2 avenue Jean Moulin, 90000 Belfort, France
[2]Bahir Dar Energy Center, Bahir Dar Institute of Technology, Bahir Dar University, Bahir Dar, Ethiopia
[3]FEMTO-ST Institute, Univ. Bourgogne Franche-Comte, CNRS, MN2S Department, 15b Avenue des Montboucons, 25000 Besançon, France

**Abstract.** In this paper, we present a new model design and parametric studies of a miniature Stirling cooler machine for on-site refrigeration. The MEMS (Microelectromechanical systems) technology is investigated to design this machine. The concept could be used to provide cooling at chip scale and mitigate hot spots in electronic devices. Whereas numerous works deal with Stirling engines at a macroscopic scale, only a few works concern miniaturized Stirling engines. Therefore, a model analysis giving insights of the impact of the technological choices and downsizing of the machine is needed. A base design model is presented. The model results lead to a cooling power of 10 mW and a Coefficient Of Performance of 1.45. A parametric study is conducted for operational and design parameters. Compared to macro-scale design, the same trend is observed for the influence of the thermal performance regenerator. Different trends from macroscopic engines were observed for hysteresis losses importance, and the choice of the working gas. The raise in power due to the raise in frequency expected for micro-scale devices is counterbalanced by the degradation of the COP due to the increase in thermofluidic losses. Squeeze film damping and finite speed losses can be neglected at this scale.

## 1 Introduction

The development of electronic appliances and their miniaturization raise the concern of cooling methods and technologies for increased high flux devices and non-uniform power dissipation. Moreover, the failure factor of electronic devices increases sharply with their operating temperature [1]. On the other hand, the development of MicroElectroMechanical Systems (MEMS) makes possible to design thermal machines at a micro-scale level. Therefore, in this paper, we investigate the modelling and design of a Stirling micro-cooler. The aimed application is to provide cooling at chip scale and mitigate hot spots in electronic

* Corresponding author: sylvie.begot@univ-fcomte.fr

devices. Whereas numerous works deal with Stirling engines or coolers at a macroscopic scale [2-3], only a few works concern miniaturized Stirling machines. The first prototype on a centimetre scale of a Stirling engine was developed by Nakajima *et al*. in 1989 [4]. It included a 0.05 $cm^3$ swept volume and delivered a power of 10 mW at 10 Hz operating between temperatures of 273 K and 373 K. In 2002, Moran patented a micro-cooler made up from a Stirling micromachine [5]. Silicon membranes, electrostatically actuated, played the role of the pistons. Several types of regenerators were tested [6]. After experimental tests between 100 and 1000 Hz, no notable difference in temperature between the chambers was observed. In 2013, Guo *et al*. [7] proposed a multiphysical modelling of a MEMS Stirling cycle cooler. The expansion and compression volumes were planned to be etched in a silicon wafer. The pistons were replaced by 2.25 mm diameter electrostatic actuated membranes. A regenerator made up of pillars was placed between the 2 volumes. The machine pressure was 2 bar. A Schmidt isothermal analysis supplemented by a loss modelling including pressure drop and regenerator effectiveness showed that the expected COP at 200 Hz was 5.2 for temperatures of 313 K for the hot sink and 288 K for the cold source. In 2015, Formosa *et al*. proposed and modelled a multiphase membrane machine for thermal energy harvesting [8-9]. It consisted of three coupled elementary phases, each composed of a 5 mm-diameter membrane which acted as a piston and transducer integrating a piezoelectric planar spiral, an expansion chamber, and a compression chamber linked by a regenerator.

To conclude, Stirling machines at macroscopic scale are a well-known technology both in engine and cooler modes, but except for the centimetric engine designed by Nakajima et *al.*, micro-scale Stirling cycles machines are not operating yet. Therefore, it seems appropriate to investigate Stirling coolers at micro-scale by developing and adapting a complete thermodynamic model to the specificity of micro-scale design. This is the main topic of the paper. The first part of the paper presents the micro-machines specific features and configuration. The second part describes the adapted adiabatic model including losses. The last part of the paper presents the base design characteristics and results. Parametric studies investigating the influence of operating parameters, design parameters, and the nature of the working gas are presented. From these results, some design guidelines for miniature engines are provided.

## 2 Micro-cooler specific features

The Stirling micro-cooler design has to be adapted for technological reasons. In this section, we describe the initial choices of the design. These choices have an impact on the model equations, for this reason, the model is described in detail after defining the micro-scale design main features. In the first place, we choose an Alpha configuration because the symmetry of the compression and expansion chambers are adapted to batch fabrication. The machine materials that can be used are those adapted to MEMS facilities. Therefore, the chosen base materials are glass and silicon [10]. Due its higher thermal conductivity, silicon is used where heat exchange is needed, while glass is used when heat exchange is detrimental. The general layout of the machine, the heat exchangers and the regenerator are presented in Fig. 1.

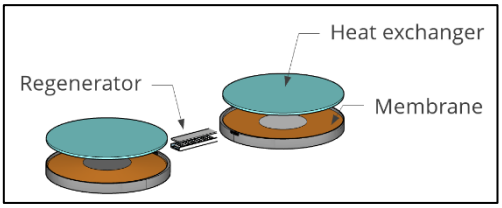


**Fig. 1.** Micro-cooler layout

Second, the pistons are not practical at microscale. Therefore, the micromachine base design consists of an engine with compression and expansion chambers swept by membranes instead of pistons. These membranes can be electrostatically actuated. This choice was also made by Moran [5] and Guo *et al*. [7]. Thus, the membrane is a hybrid membrane made from a centre silicon disk embedded in RTV silicone (Fig. 2). More details on the design and fabrication are given in Diallo *et al*.'s work [11] where the technological feasibility of this membrane was established.

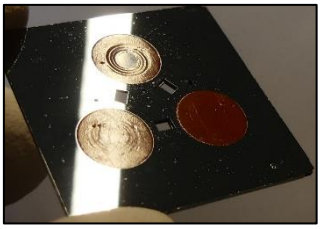

**Fig. 2.** Hybrid Membranes

The membrane swept volume is only a fraction of the cylinder volume. As in macro-scale design, a clearance volume separates the membrane top dead centre position from the chamber maximal height. The hot and cold heat exchangers are made from ducts etched in the silicon plate closing the chambers. In macro-scale design, the regenerator is usually made from woven screens, metal felts or involute foils. In our case, these technologies are not applicable, therefore we choose to use an array of pillars to fulfil the function of regeneration. Silicon is chosen as the material of the pillars to promote heat transfer, glass is chosen for the walls to limit the heat transfer from the hot part of the machine to the cold part. The fabrication of the regenerator includes a first step where a glass wafer and silicon wafer are assembled by anodic bonding, then the pillars are etched by Deep Reactive Ion Etching (DRIE). More details on the design, fabrication and CFD modelling of the regenerator can be found in references [12-13] where the technological feasibility of this kind of regenerator was established.

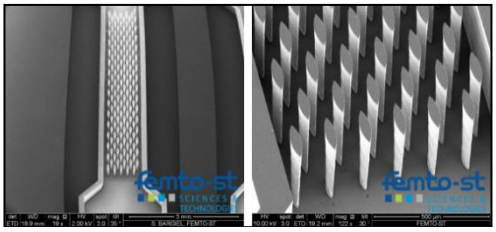

**Fig. 3.** Regenerator

# 3 Model

## 3.1 Principle

The model is based on the developments presented by Urieli and Berchowitz [14]. The "simple" analysis is used and adapted to the specific configuration of micro-coolers. The first concern is the use of membranes instead of pistons. Therefore, shuttle heat losses, mass leakage losses and piston friction losses are not considered. The swept volume is only a fraction of the chamber volume. The second concern is the buffer or bounce space volume.

Due do the miniaturization of the machine and the membrane fragility, a bounce space volume is designed and its volume is kept to a minimum. The third concern is the specific geometry of the regenerator. A specific correlation different from those established for woven screens has to be used. We make the hypothesis that conduction losses are limited to the regenerator walls. Last, we investigated squeeze film damping as the miniaturization may lead to this phenomenon. Indeed, as the volume forces that work on a machine vary in direct proportion to the cube of the length, surface forces that may be negligible at a macroscopic scale may play an important role in a micromachine [15].

### 3.2 Equations

The cooling power $\dot{Q}_{in}$ of the micro-cooler is defined as:

$$\dot{Q}_{in} = \dot{Q}_k - \dot{Q}_{rl} - \dot{Q}_{wrl} \tag{1}$$

where $\dot{Q}_k$ is the net thermal power exchanged at the cold heat exchanger, $\dot{Q}_{rl}$ is the thermal power resulting from the regenerator efficiency, and $\dot{Q}_{wrl}$ is the thermal power due the conduction between the cold and hot parts of the machine [14].
The Coefficient Of Performance is computed as the ratio of the cooling power to the absorbed mechanical power:

$$COP = \frac{\dot{Q}_{in}}{\dot{W}_{mech}} \tag{2}$$

The absorbed mechanical power is determined as the power yielded by the ideal adiabatic analysis $\dot{W}_{ad}$ plus the fluid friction losses $\dot{W}_{fr}$ , the hysteresis losses in the bounce space $\dot{W}_{hys}$, the finite speed losses of the membrane $\dot{W}_{fs}$ and the squeeze film damping losses $\dot{W}_{sf}$:

$$\dot{W}_{mech} = \dot{W}_{ad} + \dot{W}_{fr} + \dot{W}_{hys} + \dot{W}_{fs} + \dot{W}_{sf} \tag{3}$$

The fluid friction losses $\dot{W}_{fr}$ are due to the fluid friction losses in the heat exchangers and in the regenerator. They are computed from the various friction factors adapted to the geometries. For the regenerator, the correlation from Vanapalli *et al.* [16] is used, for the heat exchangers, the correlation established for flows at steady-state in channels of rectangular cross-section are used.
The hysteresis losses are computed as:

$$\dot{W}_{hys} = \sqrt{\frac{1}{32}\omega\gamma^3(\gamma-1)T_{wb}Pk_g\left(\frac{\Delta V_b}{V_b}\right)^2 A_{wg,b}} \tag{4}$$

where $\dot{W}_{hys}$, $\omega$, $\gamma$, $T_{wb}$, $\Delta V_b$, $V_b$ and $A_{wg,b}$ denote the hysteresis power losses, the angular speed of the machine, the specific heat ratio, the bounce space wall temperature, the bounce space mean pressure, the variation of the bounce space volume, the total bounce space volume, and the wetted area of the bounce space respectively [14]. We make the hypotheses that the bounce wall temperature is the same as the cold source temperature $T_{cold}$ and that the mean pressure is the same as the machine mean pressure.
The finite speed losses $\dot{W}_{fs}$ are computed following the works of Costea et al. [17]. The losses due to finite speed of the membranes are evaluated from:

$$\dot{W}_{fs} = \left[\oint_{cycle} \Delta P_{fs} dV\right] f \tag{5}$$

where $f$ is the frequency of operation and $\Delta P_{fs}$ is computed as:

$$\Delta P_{fs} = \frac{1}{2}\left(P\frac{a v_{m,c}}{c_c} + P\frac{a v_{m,e}}{c_e}\right) \quad (6)$$

where $v_m$ is the membrane mean speed, $c$ is the average molecular speed $c = \sqrt{3RT}$, and $a = \sqrt{3\gamma}$.

Th squeeze film losses analysis aim is to check that during the displacement between the expansion and compression spaces, the gas can escape the chambers. The squeeze number $\sigma$ is defined as [15]:

$$\sigma = \frac{12\mu r_m^2 \omega}{P z^2} \quad (7)$$

where $\mu$ is the gas dynamic viscosity, $r_m$ is the characteristic length of the device, in our case the radius of the membrane, $P$ the mean pressure, and $z$ is the height of the film. In our case, $z$ is chamber height. When $\sigma$<<1, the Reynolds equation holds and the squeeze film damping force coefficient $D$ for a circular plate can be written as:

$$D = \frac{3\pi}{2z^3}\mu r_m^4 \quad (8)$$

Then, the damping force can be computed, and from its expression, we derive the losses:

$$\dot{W}_{sf} = \left[\frac{\omega}{2}\frac{D V_{swc}^2}{\pi r_m^4}\right] f \quad (9)$$

where $V_{swc}$ is the membrane swept compression volume.

In order to assess the performance of the micro-cooler, the efficiency $\eta$ is defined as the ratio of the $COP$ to the ideal $COP_i$ of a machine operating on the Carnot cycle:

$$\eta = \frac{COP}{COP_i} \quad (10)$$

with

$$COP_i = \frac{T_{cold}}{T_{hot} - T_{cold}} \quad (11)$$

where the $T_{cold}$ is the cold source temperature, $T_{hot}$ the hot sink temperature.

### 3.3 Base design characteristics and results

Using this model, a base design is proposed. Each chamber diameter is 5 mm. The membrane thickness is 0.2 mm and its maximal deflection is 0.2 mm. The swept volume is 2.75 mm$^3$ corresponding to 70% of the cylinder volume. The regenerator length is 2 mm and its porosity 0.8. Heat exchangers are made from 6 ducts of 2.5 mm length. The geometric characteristics and operational parameters are presented in the Table 1. These characteristics lead to a 10.6 mW cooling power machine with a COP of 1.45 (Table 2) at 100 Hz. In order to derive some general analysis, dimensionless losses for the main contributors are computed: mechanical losses values are divided by the mechanical power $\dot{W}_{mech}$ and the thermal losses are divided by the cooling power $\dot{Q}_{in}$. The resulting dimensionless variables and results are displayed in Table 3. An analysis of the losses repartition shows that the regenerator is a key component of the performance, like in macroscopic machines. Regenerator thermal efficiency is a main contributor to the losses, and so are the thermal conduction losses in its walls. Fluid friction is also a major concern at both scales. Hysteresis losses are very high in this miniaturized Stirling machine, as compared to macroscopic machines due to the minimisation of the bounce space volume. Therefore, careful design of the bounce space should be carefully studied to minimize their impact. Both finite speed and squeeze film damping losses are negligible in this base design scale.

**Table 1.** Base design main parameters

| Parameter | Symbol | Unit | Values |
|---|---|---|---|
| **General** | | | |
| Gas | - | - | Air |
| Mean pressure | $P$ | MPa | 0.15 |
| Hot sink temperature | $T_{hot}$ | K | 313 |
| Cold source temperature | $T_{cold}$ | K | 288 |
| Frequency | $f$ | Hz | 100 |
| Phase angle | $\alpha$ | degrees | 90 |
| **Chambers** | | | |
| Membrane diameter | $d_m$ | mm | 5 |
| Membrane stroke | $s$ | mm | 0.4 |
| Chamber height | $z$ | mm | 0.23 |
| Swept volume | $V_{swc}$ | $mm^3$ | 2.75 |
| **Bounce space** | | | |
| Volume | $V_b$ | $mm^3$ | 13.7 |
| Volume variation | $\Delta V_b/V_b$ | % | 20 |
| Height | - | mm | 0.7 |
| **Cold and hot heat exchangers** | | | |
| Number of ducts | - | - | 6 |
| Length | $L_{h,k}$ | mm | 2.5 |
| Width | - | mm | 0.4 |
| Height | - | mm | 0.075 |
| **Regenerator** | | | |
| Length | $L_r$ | mm | 2 |
| Porosity | $\psi$ | - | 0.8 |
| Internal width | - | mm | 0.5 |
| Internal height | - | mm | 0.1 |
| Wall thickness | - | mm | 0.05 |
| Wall thermal conductivity | $k_r$ | $W.m^{-1}.K^{-1}$ | 1 |

**Table 2.**Base design main results

| | Symbol | Unit | Values |
|---|---|---|---|
| **Power and efficiency** | | | |
| Cooling power | $\dot{Q}_{in}$ | mW | 10.61 |
| Mechanical power | $\dot{W}_{mech}$ | mW | 7.32 |
| COP | COP | - | 1.45 |
| Efficiency | $\eta$ | % | 12.6 |
| **Losses** | | | |
| Regenerator efficiency | $\dot{Q}_{rl}$ | mW | 2.53 |
| Regenerator conduction | $\dot{Q}_{wrl}$ | mW | 1.05 |
| Pressure drop | $\dot{W}_{fr}$ | mW | 0.58 |
| Hysteresis | $\dot{W}_{hys}$ | mW | 2.32 |
| Membrane finite speed | $\dot{W}_{fs}$ | mW | $1.48\text{x}10^{-4}$ |
| Squeeze film damping | $\dot{W}_{sf}$ | mW | $5.60\text{x}10^{-6}$ |

**Table 3.** Base design dimensionless losses

| Dimensionless losses | Symbol | Values |
|---|---|---|
| Regenerator efficiency | $\dot{Q}_{rl,dless} = \dot{Q}_{rl}/\dot{Q}_{in}$ | 0.24 |
| Regenerator conduction | $\dot{Q}_{wrl,dless} = \dot{Q}_{wrl}/\dot{Q}_{in}$ | 0.10 |
| Pressure drop | $\dot{W}_{fr,dless} = \dot{W}_{fr}/\dot{W}_{mech}$ | 0.08 |
| Hysteresis | $\dot{W}_{hys,dless} = \dot{W}_{hys}/\dot{W}_{mech}$ | 0.32 |

# 4 Parametric analysis

## 4.1 Effect of operating parameters

In this paragraph, the impact of the operating parameters on the micro-cooler performance is investigated. First, we studied the impact of the cold source temperature. On the considered range 273 K-298 K, the temperature difference between heat source and sink diminishes, thus, the machine cooling power raises from 8.2 to 12.2 mW (Fig. 4a). Therefore, the cooling capacity per $cm^2$ of cooled surface varies from 41.7 $mW.cm^{-2}$ to 62.1 $mW.cm^{-2}$. The COP also raises due to the decrease in the heat losses that depend on the temperature difference (Fig. 4b). The ideal coefficient of performance $COP_i$ sharply raises as the temperature difference increases (Fig. 4c). As the mechanical losses do not diminish with the temperature difference, the micro-cooler efficiency decreases from 0.17 to 0.12.

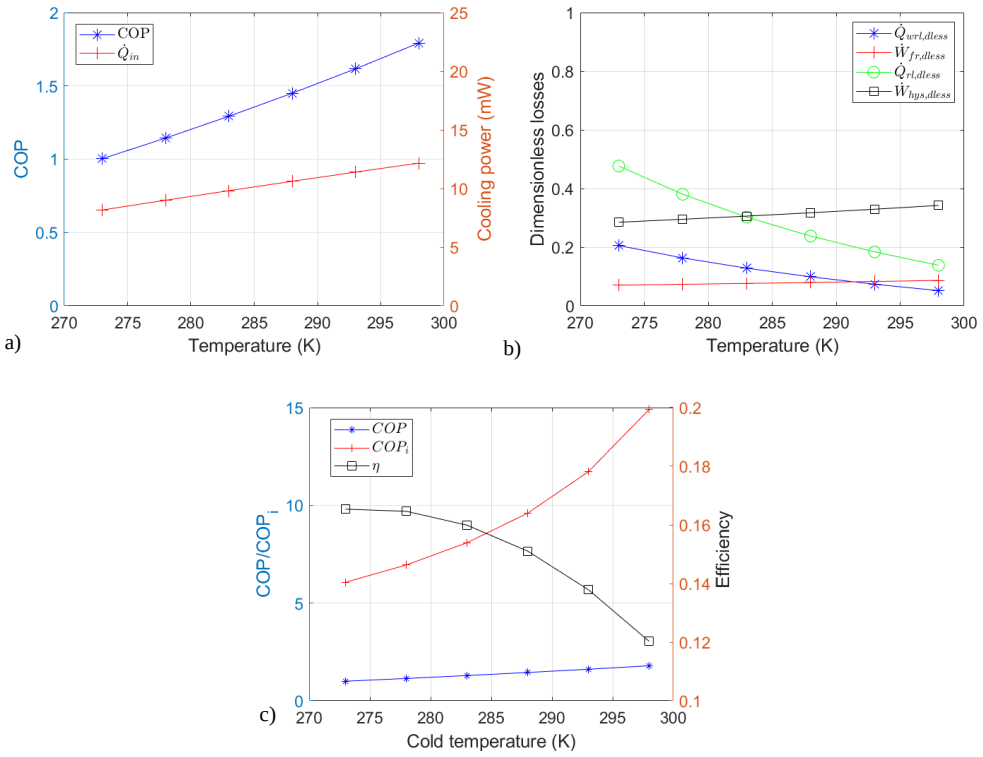


**Fig. 4.** Impact of the cold source temperature

Second, the analysis of the performances with the frequency variation was made (Fig. 5). As expected, the cooling power raises but the COP presents a maximum at 75 Hz (Fig. 5a). The raise in regenerator efficiency losses is partly responsible for the decrease in the COP when the frequency raises above 75 Hz (Fig. 5b). Whereas the high frequency leads to an increase in power, it is also detrimental to heat exchange. The fluid friction losses also raise with the increase in frequency and thus in gas velocity. The evolution of the COP with the cooling power presents a maximum at 75 Hz (Fig. 5c). At this frequency, a compromise between COP and efficiency is achieved. Therefore, the machine miniaturization does not lead to a large increase in the optimal operational frequency compared to macroscopic engines that operate at about 50 Hz, and this is mainly due to thermofluidic phenomena.

Third, as in macroscopic machines, a raise in pressure directly leads to an approximately linear raise in cooling power (Fig. 6a). The increase in losses with pressure is mainly due to thermal efficiency of the regenerator (Fig. 6b). However, the machine COP remains stable in the pressure range $1x10^5$ Pa and $4x10^5$ Pa. Operation above this pressure would lead to technological challenges, therefore the influence of higher pressures was not investigated in this study.

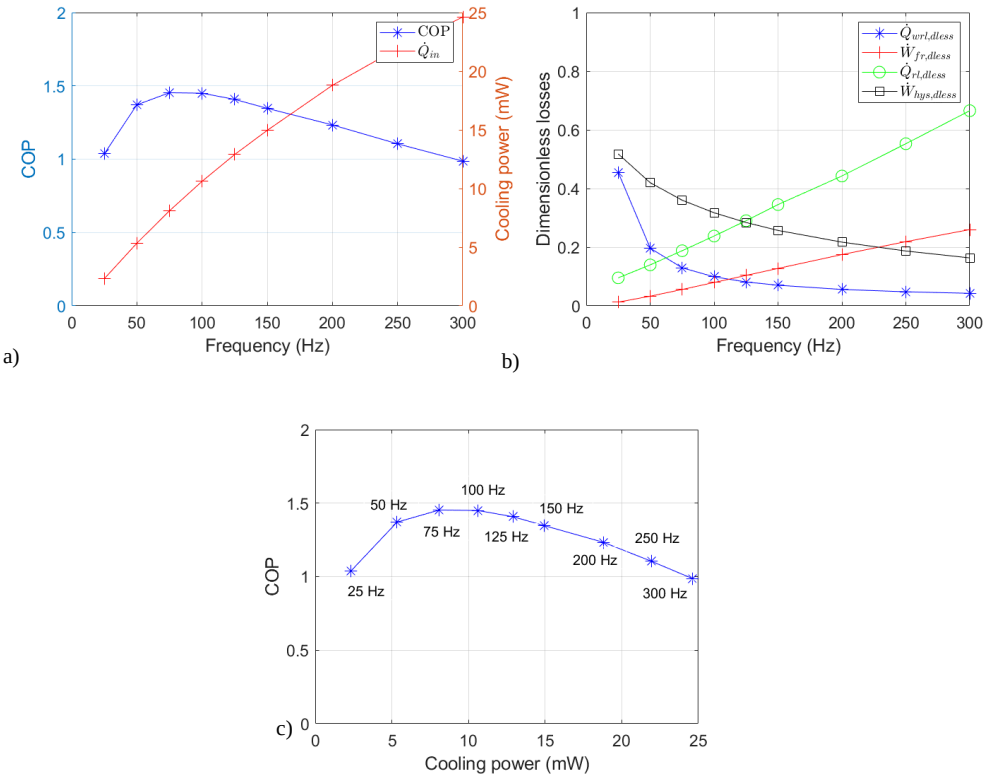


**Fig. 5.** Impact of the frequency

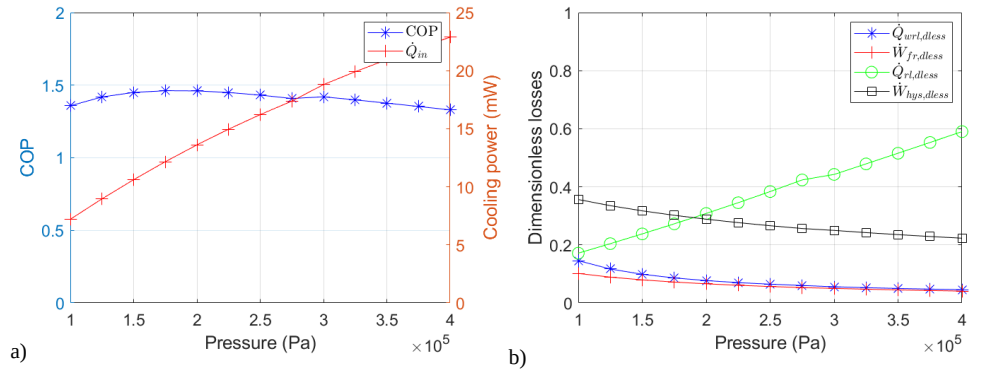


**Fig. 6.** Impact of the pressure

## 4.2 Effect of some design parameters

In this paragraph, the influence of some of the geometric design parameters is studied. As the regenerator efficiency and conduction losses are the first two main losses of the base design model (Table 2), regenerator geometry was studied. First, the impact of the regenerator length is studied. The cooling power increases with the regenerator length (Fig. 7a). The COP variation with the regenerator length presents a sharp raise, a maximum at 3 mm, then a slight

decrease. The observation of the losses (Fig. 7b) shows that a short regenerator leads to high regenerator thermal efficiency losses and high conduction losses. Indeed, a short regenerator does not enable all heat exchange between the gas and the regenerator pillars to take place during the cycle. The conduction losses are high when the regenerator length is small. Increasing the length leads to an increase in cooling power. On the other hand, the higher length values lead to an increase in the friction losses. These phenomenon account for the shape or the cooling power and COP curves.

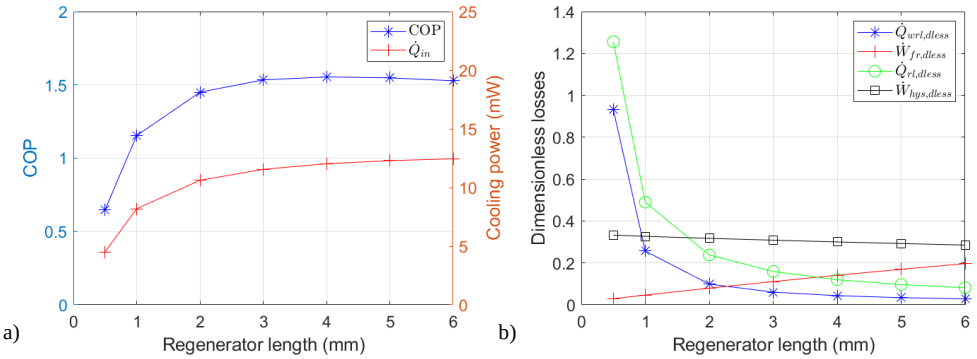


**Fig. 7.** Impact of the regenerator length

The same analysis was made with the variation of the regenerator porosity. For a 2 mm-long regenerator, the COP slightly decreases of 7% from 1.46 to 1.36 over a porosity range of 0.7 to 0.9 (Fig. 8a). On this range, the power decreases of 14% from 11.2 to 9.6 mW. The observation of the main losses (Fig. 8b) shows that the regenerator thermal efficiency losses raise when the porosity is higher but on the other hand friction losses decrease. This accounts for the shape of the COP and cooling power curves.

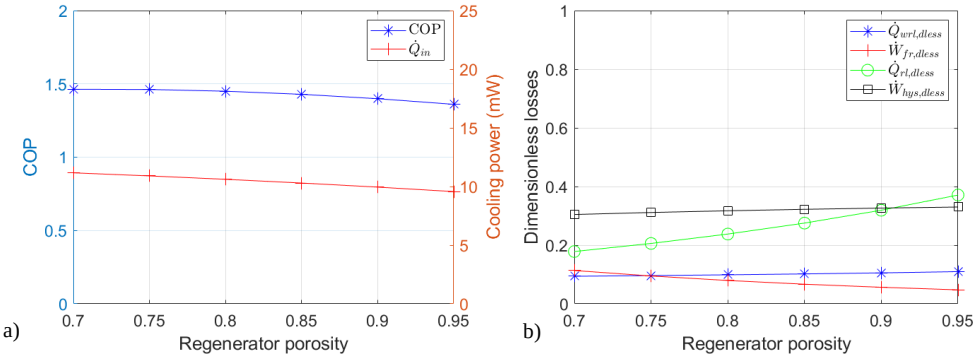


**Fig. 8.** Impact of the regenerator porosity

For the base design, hysteresis losses in the bounce space are also one of the main losses (Table 2). As they depend on the bounce space volume relative variation $\Delta V_b/V_b$ during the cycle (4), their amplitude is large when this volume relative variation is high. In macroscopic engines, the bounce space volume is usually designed large, and as a consequence the relative variation is small. However, as our aim is to have a miniature machine, this will not be necessarily the case in our design. Thus, we studied the COP and cooling power of the micro-cooler with the bounce space volume variation. The cooling power remains stable with the

relative variation, but the machine COP decreases of 34 % with $\Delta V_b/V_b$ (Fig. 6a). We observe that, for the base design, the hysteresis losses overcome the fluid friction losses for a volume variation of 6% (Fig. 6b). A large bounce space volume leading to small relative variations during the cycle is beneficial, therefore, when designing a micro-cooler, the bounce space volume should be carefully studied.

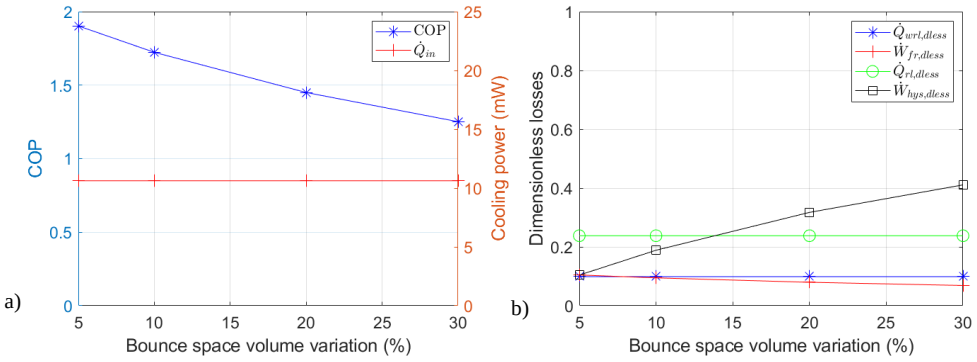


**Fig. 9.** Impact of the bounce space volume

## 4.3 Effect of the working gas

Finally, we simulated the performance of the micro-cooler using helium and hydrogen as working gases instead of air. Helium is a frequent working gas for macroscopic engines due to its high thermal conductivity. Hydrogen properties are also interesting and miniature engines need a small mass of hydrogen reducing hydrogen safety concerns. The cooling power and COP for the three gases are plotted in Fig. 10a. Helium appears to be the better choice regarding the cooling power, but its COP is reduced due to high hysteresis losses (Fig. 10b) linked to its high specific heat ratio γ. Air presents the better COP but its cooling power is reduced by high regenerator efficiency losses. Hydrogen present intermediate performances in cooling power and COP.

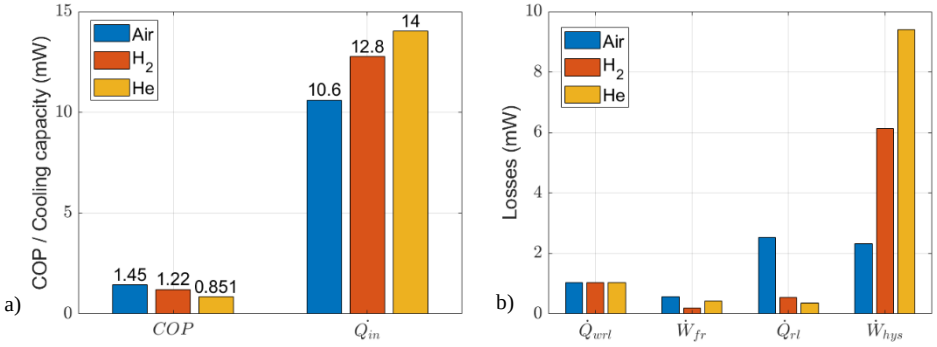


**Fig. 10.** Impact of the working gas

## 5 Conclusion

In this paper, we investigate the modelling and design of a Stirling micro-cooler that could be used to provide cooling at chip scale and mitigate hot spots in electronic devices. This MEMS technology leads to the use of specific materials and geometries that are not common in macroscopic machines. After adaptation of the model to these specific characteristics, we proposed a base design machine. We performed a parametric analysis in order to analyse the performance of the machine with the variation of operational parameters, some geometric parameters and working gas. Compared to macro-scale design, the same trend was observed for the influence of the thermal performance regenerator. However, different trends from macroscopic engines were observed. The raise in power due to the raise in frequency expected for micro-scale devices is counterbalanced by the degradation of the COP due to the increase in thermofluidic losses. Hysteresis losses in the bounce space are also of high amplitude due to the small size if this volume. The choice of the working gas between air, helium and hydrogen has to be adapted to the objectives in cooling power or COP. Both finite speed and squeeze film damping losses are negligible for the investigated machine size.

This work has been supported by the EIPHI Graduate School (contract ANR-17-EURE-0002) and the Region Bourgogne-Franche-Comté.

## References

[1] S. Sohel Murshed and C. Nieto de Castro, *Renew. Sust. Energy. Rev.*, **78**, pp. 821–833, (2017). https://www.sciencedirect.com/science/article/pii/S1364032117305944
[2] D. Thombare and S. Verma, *Renew. Sust. Energy. Rev.*, **12**, pp. 1 – 38, (2008). http://-www.sciencedirect.com/science/article/pii/S1364032106000906
[3] M. Z. Getie, F. Lanzetta, S. Bégot, B. T. Admassu, and A. A. Hassen, *Int. J. Refrig.*, **118**, pp 173-187, (2020). http://www.sciencedirect.com/science/article/pii/-S0140700720302619
[4] N. Nakajima, K. Ogawa, and I. Fujimasa, *Sens. Actuator A Phys*, **20**, pp. 75 – 82, (1989). http://www.sciencedirect.com/science/article/pii/0250687489871045
[5] M. Moran, Patent, May 14, 2002, US Patent 6,385,973. https://www.google.com/-patents/US6385973
[6] M. Moran, D. Wesolek, B. Berhane, and K. Rebello, *2nd International Energy Conversion Engineering Conference*, p. 5611 (2004).
[7] D. Guo, J. Gao and S.-C. Yao, *J. Heat Transfer*, **135**, pp 111003-111010 (2013).
[8] F. Formosa and L. Fréchette, *J. Phys. Conf. Ser.*, **660**, pp. 012071, (2015).
[9] T. Avetissian, É. Leveillé, M.-A. Hachey, F. Formosa, and L. Fréchette, *J. Phys. Conf. Ser.*, **1407**, pp. 012041, (2019).
[10] M. J. Madou, *Fundamentals of microfabrication: the science of miniaturization*. (CRC press, 2002).
[11] A. D. Diallo, *Contribution to the design and construction of a thermal micromachine with Stirling cycle,* PhD of University Bourgogne Franche-Comté, (2019).
[12] E. Dellali, S. Bégot, F. Lanzetta, E. Gavignet, R. Chutani, and J. Rauch, *17th International Stirling Engine Conference and Exhibition,* pp. 190 – 200 (2016).
[13] E. Dellali, S. Bégot, F. Lanzetta, E. Gavignet, and J. Rauch, *Exp. Therm. Fluid Sci.*, **103**, pp. 394–405, (2019).
[14] I. Urieli and D. M. Berchowitz, *Stirling cycle engine analysis*. (Bristol: Adam Hilger, 1984).
[15] M. Bao and H. Yang, *Sens. Actuator A Phys.*, **136**, pp. 3 – 27, (2007), http://-www.sciencedirect.com/science/article/pii/S0924424707000118

[16] S. Vanapalli, H. Brake, H. Jansen, J. Burger, H. Holland, T. Veenstra, and M. Elwenspoek, *J. Micromech. Microeng.*, **17**, p. 1381, (2007). http://stacks.iop.org/0960-1317/17/i=7/a=021
[17] M. Costea, S. Petrescu, and C. Harman, *Energy Convers. Manag.*, **40**, no. 15-16, pp. 1723–1731, 1999.

## Nomenclature

| | |
|---|---|
| $A_{wg}$ | wetted area, $m^2$ |
| $c$ | average molecular speed, $m.s^{-1}$ |
| COP | Coefficient Of Performance |
| D | squeeze film damping coefficient, $kg.s^{-1}$ |
| $f$ | frequency, Hz |
| k | thermal conductivity, $W.m^{-1}.K^{-1}$ |
| P | pressure, Pa |
| $\dot{Q}_{in}$ | cooling power, W |
| $\dot{Q}_k$ | power exchanged at the cold heat exchanger, W |
| $\dot{Q}_{rl}$ | regenerator power losses, W |
| $\dot{Q}_{wrl}$ | regenerator wall conduction losses, W |
| $r$ | radius, m |
| $T$ | temperature, K |
| $v$ | velocity, $ms^{-1}$ |
| $V$ | volume, $m^3$ |
| $\dot{W}_{ad}$ | adiabatic analysis power, W |
| $\dot{W}_{fr}$ | fluid friction losses, W |
| $\dot{W}_{fs}$ | membrane finite speed losses, W |
| $\dot{W}_{hys}$ | hysteresis losses, W |
| $\dot{W}_{mech}$ | absorbed mechanical power, W |
| $\dot{W}_{sf}$ | squeeze film damping losses, W |
| $z$ | chamber height, m |

### Greek symbols

| | |
|---|---|
| $\eta$ | efficiency |
| $\gamma$ | specific heat ratio |
| $\psi$ | dimensionless regenerator porosity |
| $\mu$ | dynamic viscosity, $Ns.m^{-2}$ |
| $\sigma$ | squeeze number |
| $\omega$ | angular speed, $rad.s^{-1}$ |

### Subscripts

| | |
|---|---|
| $b$ | bounce space |
| c | compression space |
| e | expansion space |
| g | gas |
| i | ideal |
| m | membrane |

| | |
|---|---|
| r | regenerator |
| swc | swept compression |
| w | wall |